Adsorption 11: 615–620, 2005

Simulation and Optimization of a Pressure Swing Adsorption System: Recovering Hydrogen from Methane

SETH P. KNAEBEL*, DAEHO KO AND LORENZ T. BIEGLER
Department of Chemical Engineering, Carnegie Mellon University, Pittsburgh, Pennsylvania 15213, USA
spk@andrew.cmu.edu

Abstract. Recent developments in the fuel cell industry have yielded an increase in expected demand for a pure hydrogen source; one attractive method for meeting this demand involves separating hydrogen from a hydrogen-methane mixture using pressure swing adsorption (PSA). In designing PSA systems, the selection of the adsorbent and operational flowsheet are the most important and limiting decisions; beyond this, implementing systematic methods to find optimal operating conditions and bed parameters is essential. These decision variables include flowrates, bed pressures, step times and bed dimensions. This research examines this PSA system via dynamic simulation and optimization; the primary purpose of the optimization is to maximize the recovery of the key components while meeting both the hydrogen purity and cyclic steady state requirements. In this study, the process model is formulated for this separation using gPROMS. The model discretizes the spatial domain, and binary variables are used to adjust the boundary conditions for the bed as the system runs through the four-step PSA cycle. Two alternative PSA cycles are simulated, optimized and compared to assess the best performance for this PSA separation.

Keywords: PSA, process simulation, process optimization

1. Introduction

The primary focus of this work is to maximize the recovery of fuel cell grade hydrogen (∼99.9%) from a 75% methane feed using pressure swing adsorption. For this purpose, computer simulations can be a valuable complement to the experimental analyses commonly used to design PSA systems, because these systems can require thousands of cycles to reach CSS. This separation is simulated using a set of partial differential and algebraic equations (PDAE's) and the axial dimension is discretized using centered finite differences. Using the Method of Lines (Schiesser, 1991), PDAEs are converted to a set of DAEs, which are solved using backward differentiation formulas (BDF) within gPROMS. gPROMS is a general purpose, equation based simulation and optimization package developed by the Centre for Process Systems Engineering at Imperial College in London, and is commercially marketed by Process Systems Enterprise. Moreover, the dynamic optimization in gPROMS allows the user to determine optimal values for design variables (bed dimensions) and operating conditions (step times, bed pressures, flowrates, etc.) simultaneously.

In the next section we present the PSA model for the hydrogen/methane separation. A brief experimental validation of the model is presented in Section 3. Section 4 then presents base case simulation results in gPROMS while Section 5 summarizes the optimization results. Section 6 then summarizes the paper and outlines future work.

2. PSA Model

The PSA model makes the following assumptions:

1. Gases obey the ideal gas law.

*To whom correspondence should be addressed.

2. There are no radial variations in temperature, pressure, or concentration.
3. Transport and physical properties are considered to be temperature independent.
4. Bed pressure is constant during the adsorption and regeneration steps.
5. Adsorption equilibrium is described by the Langmuir isotherm.
6. Adsorption rate is approximated by a linear driving force (LDF).

The component mass balance and overall mass balance for this system are presented below in Eqs. (1) and (2), respectively. The overall mass balance accounts for a variable superficial velocity over the bed for this bulk separation. Here D_x is the dispersion coefficient (m^2/s) and i is the component ($1 = CH_4$, $2 = H_2$), y_i is the gas phase mole fraction, z is the axial position (m), t is time (s), u is the superficial gas velocity (m/s), R is the gas constant (J/mol/K), T and P are the temperature of the gas (K) and the total pressure (Pa) within the bed, respectively. ε_{bed} is the bed void, q_i is loading of component i, ρ_{gas} and ρ_{bed} are the gas and bed densities. The axial dispersion coefficient in Eq. (1) depends on the molecular diffusivity, adsorbent particle radius, and the velocity, and is defined in Eq. (3). The energy balance is presented in Eq. (4). ΔH_i is the heat of adsorption for component i, h is the heat transfer coefficient of the column wall.

$$-D_x\left[\frac{\partial^2 y_i}{\partial z^2} + 2T\left(\frac{\partial y_i}{\partial z}\right)\left\{\frac{\partial}{\partial z}\left(\frac{1}{T}\right)\right\}\right] + \frac{\partial y_i}{\partial t} + u\frac{\partial y_i}{\partial z} + \frac{RT}{P}\frac{1-\varepsilon_{\text{bed}}}{\varepsilon_{\text{bed}}}\rho_{\text{particle}}\left(\frac{\partial q_i}{\partial t} - y_i\sum_{i=1}^{n}\frac{\partial q_i}{\partial t}\right) = 0 \tag{1}$$

$$\frac{\partial u}{\partial z} + \frac{1}{P}\frac{\partial P}{\partial t} + T\left\{-D_x\frac{\partial}{\partial z^2}\left(\frac{1}{T}\right) + \frac{\partial}{\partial t}\left(\frac{1}{T}\right) + u\frac{\partial}{\partial z}\left(\frac{1}{T}\right)\right\} + \frac{\rho_{\text{particle}}RT}{P}\frac{1-\varepsilon_{\text{bed}}}{\varepsilon_{\text{bed}}}\sum_{i=1}^{n}\frac{\partial q_i}{\partial t} = 0 \tag{2}$$

$$D_{\text{axial}}(Z) = 0.7D_m + \frac{1}{2}D_{\text{particle}}u(z) \tag{3}$$

$$(\varepsilon_t\rho_{\text{gas}}C_{\text{pg}} + \rho_{\text{bed}}C_{\text{ps}})\frac{\partial T}{\partial t} + \rho_{\text{gas}}C_{\text{pg}}\varepsilon_{\text{bed}}u\frac{\partial T}{\partial z} - K_L\frac{\partial^2 T}{\partial z^2} - \rho_{\text{bed}}\sum_{i=1}^{n}\Delta H_i\frac{\partial q_i}{\partial t} + \frac{2h}{R_{\text{bed}}}(T - T_{\text{wall}}) = 0 \tag{4}$$

Table 1. Isotherm parameters for hydrogen and methane on activated carbon.

	a_1 (mol/(kg-MPa))	a_2 (1/K)	b_1 (1/MPa)	b_2 (1/K)
Methane	0.00846	−0.2155	0.0004066	−0.010604
Hydrogen	−0.00003786	−0.01815	2.2998	−0.05993

The adsorption rate is represented by the linear driving force (LDF) in the model, which is presented in Eq. (5). In this equation, q_i^* is the equilibrium loading for component i, and k_i is the LDF coefficient, the approximate range for which is determined using the pore or effective diffusivity and the Glueckauf approximation. The value of this parameter is adjusted using a dynamic experimental verification process, which is outlined below. The heat of adsorption is derived using the Clausius-Clapeyron, Eq. (6), in conjunction with the temperature dependent isotherm parameters.

$$\frac{\partial q_i}{\partial t} = k_i(q_i^* - q_i) \tag{5}$$

$$\left[\frac{d\ln P}{d(1/T)}\right]_q = -\frac{\Delta H}{R} \tag{6}$$

$$q_i^* = \frac{a_i P_i}{1 + \sum_{i=1}^{n} b_i P_i} \qquad \begin{matrix} a_i(T) = a_{1,i}\exp(a_{2,i}T) \\ b_i(T) = b_{1,i}\exp(b_{2,i}T) \end{matrix} \tag{7}$$

Activated carbon was chosen as the adsorbent for this system because of the preferential adsorption behavior of the components involved in the separation. The competitive adsorption behavior is described by the Langmuir Isotherm, and presented in Eq. (7). P_i is the partial pressure of species i, and a_i and b_i are the corresponding Langmuir coefficients. A simple nonlinear regression was performed to estimate the parameters describing the temperature dependence of the isotherm relations. Table 1 presents the results of this

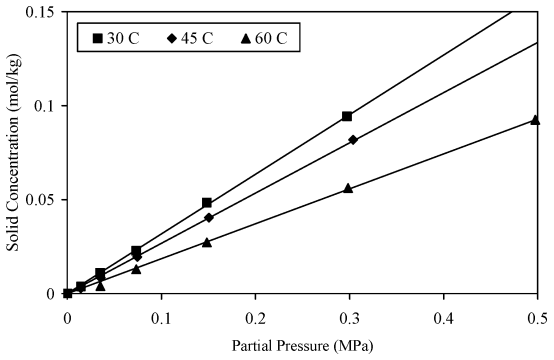

Figure 1. Hydrogen isotherm with Langmuir fit.

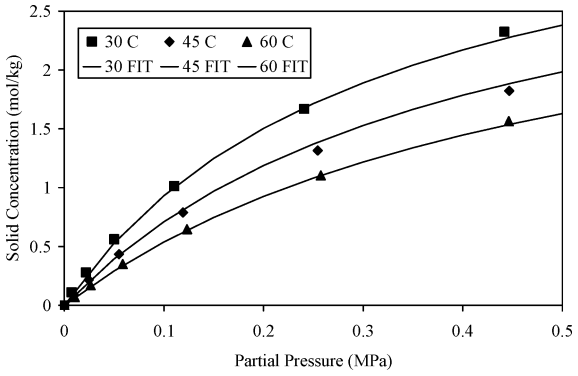

Figure 2. Methane isotherm with Langmuir fit.

nonlinear regression and the corresponding isotherm data is presented in Figs. 1 and 2.

3. Experimental Verification

Here we compare simulation results to experimental results in order to both adjust the dispersion and LDF coefficients and ensure that the model accurately predicts the physical behavior exhibited by bench-scale laboratory equipment. Similar in purpose to a desorption breakthrough test, the experimental setup developed by Prof. M. Eic and colleagues at the University of New Brunswick involves a packed bed with a high pressure binary mixture of 75% methane and 25% hydrogen at equilibrium on the activated carbon adsorbent. Hydrogen is then fed to the column and the methane concentration is measured at the outlet. These outlet concentration profiles are then compared using feed flowrates of 100 and 500 mL/min. The LDF coefficient was adjusted to the value of 0.131 1/s and the correlation for the dispersion coefficient, as defined in Eq. (3), was confirmed using a value of 10^{-7} for molecular diffusivity. The simulation and experimental results are presented in Fig. 3.

4. Simulation to Cyclic Steady State

The mathematical model describes a bench-scale, single-bed pressure swing adsorption system that undergoes a simple four-step cycle; the four steps making up each cycle are: (1) pressurization, (2) adsorption, (3) depressurization, and (4) regeneration. During the first step, the bed is pressurized with either a feed pressure (25% hydrogen, 75% methane, used for cycle A) or recycled product at ambient temperature (used for cycle B). In the second step, the feed mixture flows into the bed at high pressure, methane continues to adsorb preferentially to the surface of the adsorbent, and purified hydrogen is released through the top of the bed. In step 3 the pressure is reduced linearly to atmospheric pressure and the methane begins to desorb from the surface of the adsorbent. In the last step, the bed is purged with hydrogen to regenerate the adsorbent and the cycle is allowed to repeat.

The behavior of the individual steps within the cycle is simulated by varying the boundary conditions of the bed, which are formulated in gPROMS using binary variables. Additional flowsheets can be considered by varying the boundary conditions imposed on

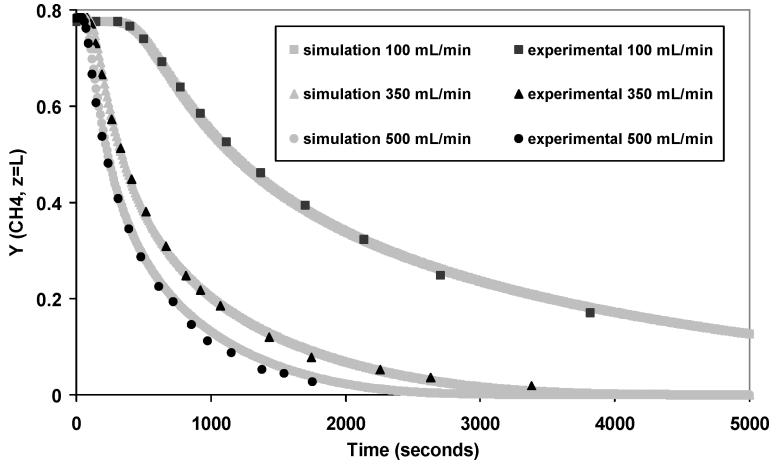

Figure 3. Product-purity simulation results.

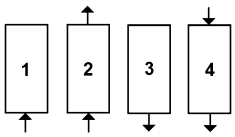

Figure 4. PSA cycle A: feed pressurization.

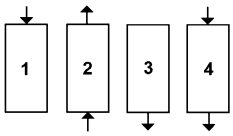

Figure 5. PSA cycle B: product pressurization.

the model equations. The boundary conditions describing the four-step PSA cycles are introduced in Table 2. The product pressurization boundary conditions are not presented here for the sake of space. The molar flow rates into and out of the ends of the bed are approximated by the differential equations listed at the bottom of Table 2. These variables are re-initialized at the beginning of each cycle, and are used in defining the performance variables discussed below.

The final set of constraints in the model is that of the performance criteria: the definitions of several variables that will be used to judge the performance of the simulated separation. In previous work, the trend was to maximize the purity of the two product streams while constraining the system to a maximum power requirement. However, the model may be optimized with respect to any number of criteria: product purity, specific power, product recovery, etc., and the remaining criteria can be implemented as constraints on the optimization. The performance criteria are presented in Eqs. (8)–(10).

$$\text{Purity}_{\text{H}_2} = \frac{\text{Product}_{\text{H}_2}}{\sum_{i=1}^{n} \text{Product}_i} \tag{8a}$$

$$\text{Purity}_{\text{CH}_4} = \frac{\text{Exhaust}_{\text{CH}_4}}{\sum_{i=1}^{n} \text{Exhaust}_i} \tag{8b}$$

$$\text{Recovery}_{\text{H}_2} = \frac{\text{Product}_{\text{H}_2} - \text{Purge}_{\text{H}_2}}{\text{Feed}_{\text{H}_2}} \tag{9a}$$

$$\text{Recovery}_{\text{CH}_4} = \frac{\text{Exhaust}_{\text{CH}_4}}{\text{Feed}_{\text{CH}_4}} \tag{9b}$$

Equations (8a) and (8b) define the purity of the two components in the current model. Equations (9a) and (9b) describe the recovery of these components. Finally, Eq. (10) shows the specific power required for the separation, where γ is the ratio of the heat capacities (C_p/C_v).

$$\text{Power} = \frac{\gamma}{\gamma - 1} RT_{\text{feed}} \left[\left(\frac{P_{\text{feed}}}{P_{\text{atm}}} \right)^{(\gamma-1)/\gamma} - 1 \right] \times u_{\text{feed}} \pi r_{\text{bed}}^2 \frac{P_{\text{feed}}}{RT_{\text{feed}}} \tag{10}$$

Here we simulate each of the pressurization schemes to cyclic steady state. The physical properties and simulation parameters are presented below in Table 3. For the feed pressurization study, the step times were all set to 20 seconds. For the product pressurization scheme, the pressurization and depressurization steps were set to 30 seconds, but the adsorption and regeneration steps were each set to 60 second durations. These step times were manually determined by running several simulations, and using the settings that yield the desired product purity. The simulation results are presented in Table 4, and are used as the basis for the optimization, which is presented in the following section.

Table 2. Boundary conditions for PSA cycle.

Pressurization (Cycle A)	Pressurization (Cycle B)	Adsorption	Depressurization	Regeneration
$y_i\|_{z=0} = y_{f,i}$	$\frac{\partial y_i}{\partial z}\|_{z=0} = 0$	$y_i\|_{z=0} = y_{f,i}$	$\frac{\partial y_i}{\partial z}\|_{z=0} = 0$	$\frac{\partial y_i}{\partial z}\|_{z=0} = 0$
$\frac{\partial y_i}{\partial z}\|_{z=L} = 0$	$y_{\text{H}_2}\|_{z=L}$ = specified $y_{\text{CH}_4}\|_{z=L} = 1 - y_{\text{H}_2}\|_{z=L}$	$\frac{\partial y_i}{\partial z}\|_{z=L} = 0$	$\frac{\partial y_i}{\partial z}\|_{z=L} = 0$	$y_{\text{H}_2}\|_{z=L}$ = specified $y_{\text{CH}_4}\|_{z=L} = 1 - y_{\text{H}_2}\|_{z=L}$
$T\|_{z=0} = T_{\text{feed}}$	$T\|_{z=0} = T_{\text{feed}}$	$T\|_{z=0} = T_{\text{feed}}$	$\frac{\partial T}{\partial z}\|_{z=0} = 0$	$\frac{\partial T}{\partial z}\|_{z=0} = 0$
$\frac{\partial T}{\partial z}\|_{z=L} = 0$	$\frac{\partial T}{\partial z}\|_{z=L} = 0$	$\frac{\partial T}{\partial z}\|_{z=L} = 0$	$\frac{\partial T}{\partial z}\|_{z=L} = 0$	$T\|_{z=L} = T_{\text{purge}}$
$\frac{\partial u}{\partial z}\|_{z=0} = 0$	$\frac{\partial u}{\partial z}\|_{z=0} = 0$	$u\|_{z=0} = u_{\text{feed}}$	$\frac{\partial u}{\partial z}\|_{z=0} = 0$	$\frac{\partial u}{\partial z}\|_{z=0} \Leftarrow$ Eq. (4)
$u\|_{z=L} = 0$	$u\|_{z=L} = 0$	$\frac{\partial u}{\partial z}\|_{z=L} = 0$	$u\|_{z=L} = 0$	$u\|_{z=L} = u_{\text{purge}}$

Table 3. Physical properties and simulation parameters.

Physical properties		CSS simulation parameters	
Bed density	4.27E+02 kg/m^3	Bed length	1 m
Bed void	0.4043	Bed radius	0.25 m
Particle density	7.16E+02 kg/m^3	Ambient pressure	0.101325 MPa
Particle radius	2.47E−03 m	Feed pressure	0.5 MPa
Pore diameter	3.00E−09 m	Feed temperature	303.15 K
Cp	1046.7 J/kg/K	Feed composition	(0.25, 0.75) (H_2, CH_4)
Viscosity	1.01E−05 kg/m/s	u_adsorption	0.1 m/s
Dx	1.00E−07 1/s	u_regeneration	−0.075 m/s
LDF (Dpore)	0.131 1/s		

Table 4. CSS simulation results.

CSS simulation results	Cycle A	Cycle B	
Number of cycles	1000	2000	Cycles
Product flowrate	13.0451	1.31122	scm/hr
H2 purity	99.9674	99.9879	%
H2 recovery	26.1364	5.00641	%
CH4 purity	80.4065	80.2815	%
CH4 recovery	100	100	%
Computational time	2719.62	4922.91	s

Table 5. Dynamic optimization results.

Optimization results	Cycle A	Cycle B	
Feed pressure	0.6	0.6	MPa
Adsorption velocity	0.104978	0.0965554	m/s
Regeneration velocity	−0.0839016	−0.0573245	m/s
H2 purity	99.85	99.85	%
H2 recovery	33.395	49.9353	%
Computational time	2248.22	1204.45	s

5. Optimization

PSA systems are typically operated at cyclic steady state (CSS), which means that the temperature, mole fraction, and solid concentration bed profiles are identical at the beginning and at the end of each cycle. In this study we apply the simultaneous tailored approach described in Biegler et al. (2004). Ko et al. (2003) showed how this approach could be applied to the gPROMS modeling environment. From the simulations presented above, the CSS bed profiles are fed to gOPT, the dynamic optimizer within gPROMS, as an initial guess at the optimal CSS condition. Within the optimization problem we impose Eqs. (11) and (13), which require that the optimal solution corresponds to a system at CSS. In addition, gOPT allows us to specify ranges for the decision and operating variables, and optimize over any performance criterion. This criterion will typically involve a combination of product recovery and specific power (operating cost). In this work, we seek to maximize the recovery of fuel-cell grade hydrogen (>99.85% purity).

$$T(z)|_{t=0} = T(z)|_{t=\text{cycle}} \quad q_i(z)|_{t=0} = q_i(z)|_{t=\text{cycle}}$$
$$y_i(z)|_{t=0} = y_i(z)|_{t=\text{cycle}} \qquad (11\text{–}13)$$

The optimal solutions determined for the two pressurization schemes are presented in Table 5. Here we have required that the hydrogen product purity be in a specified range and have maximized the hydrogen recovery. Because this approach yielded identical product purities in the two pressurization schemes considered, we can make a fundamental comparison between the two cycles. It is clear that the product pressurization scheme (Cycle B) provides a higher hydrogen recovery. This suggests that it is the more efficient separation cycle. More information on the optimization and details on the simulation and optimization strategies and results can be found in Knaebel (2004) and Ko et al. (2003).

6. Conclusions

A model has been constructed to predict the behavior of a specific bulk separation. The experimental

verification suggests that this will prove a useful tool in aiding in cycle selection, and optimization capabilities present the opportunity to find optimal operating and decision variables. gPROMS has proven to be an effective vehicle for PSA simulation and optimization in this case. The framework allows for a relatively quick analysis of a variety of simple PSA systems. One minor limitation to these results is that the LDF coefficient is considered constant. The next step in this research is to allow the LDF coefficient to vary with changes in temperature, pressure, and concentration. It will be expanded to consider a ternary feed stream, and include a second layer of a different adsorbent. Our colleagues at the University of New Brunswick will continue using and updating this model, where a preliminary comparison showed excellent agreement with 4-step PSA experimental results. However, when implementing gPROMS, the user is limited in the choice of numerical solvers and the optimization strategy. Oftentimes, more complicated systems involving multiple beds and bed-to-bed interactions (such as pressure equalization steps) will require a more specialized approach. These are explored in greater detail in Biegler et al. (2004).

References

Biegler, L.T., Ling Jiang, and V.G. Fox, "Recent Advances in Simulation and Optimal Design of Pressure Swing Adsorption Systems," *Separation and Purification Reviews*, **33**(1), 1–39 (2004).

Knaebel, Seth P., "Simulation and Optimization of Pressure Swing Adsorption Systems: Recovering Hydrogen From Methane," M.S. Thesis, Carnegie Mellon University, 2004.

Ko, D., R. Siriwarndane, and L.T. Biegler, "Optimization of a Pressure-Swing Adsorption Process Using Zeolite 13X for CO2 Sequestration," *I&EC Research*, **42**(2), 339–348 (2003).

Ruthven, D.M., S. Farooq, and K.S. Knaebel, *Pressure Swing Adsorption*, VCH Publishers, New York, 1994.

Schiesser, W.E., *The Numerical Method of Lines*, Academic Press, New York, 1991.